Green Chemistry

PAPER

View Article Online
View Journal | View Issue

Cite this: *Green Chem.*, 2024, **26**, 2712

Reducing the environmental footprint of solid-electrolytes - a green synthesis route for LATP†

Melanie Rosen, [a] Philipp Hecker,[a] Markus Mann, [a] Qianli Ma, [a] Jürgen Peter Gross, [b] Ruth Schwaiger,[b,e] Olivier Guillon, [a,c] Dina Fattakhova-Rohlfing[a,c,d] and Martin Finsterbusch [a,c]*

Received 1st September 2023,
Accepted 12th January 2024

DOI: 10.1039/d3gc03293k

rsc.li/greenchem

Lithium aluminium titanium phosphate $Li_{1.5}Al_{0.5}Ti_{1.5}(PO_4)_3$ (LATP) is a promising and intensively studied solid electrolyte for the development of ceramic solid-state batteries. LATP has competitive Li-ion conductivity at room temperature, very high oxidation stability, is non-flammable, cheap and environmentally friendly. LATP can be produced in large quantities by a solution-assisted solid-state process, which can be easily scaled up for industrial applications. We show that LATP synthesis can be further simplified, reducing synthesis time, lowering energy consumption, and most importantly, reducing the environmental footprint. The core of this approach is the use of $AlPO_4$ as Al source instead of aluminium acetate. This reduces the use of H_3PO_4 in the reaction and reduces the amount of organic components, resulting in a CO_2-free synthesis. In addition, our approach allows for direct sintering without the need for high-energy calcination steps, reducing CO_2 emissions by 48% during processing. The resulting LATP exhibits very high phase purity and a homogenous microstructure, resulting in a total ionic conductivity of 0.62 mS·cm^{-1} at room temperature with an activation energy of 0.33 eV.

Introduction

Solid-state electrolytes are being intensively investigated as a possible alternative to liquid electrolytes in lithium-ion batteries. Among the numerous classes of materials, ceramic solid electrolytes are particularly attractive due to their non-flammability, relatively high ionic conductivity at room temperature and high chemical stability in air, leading to potentially very high intrinsic safety of the batteries.[1] Unlike conventional lithium-ion batteries, which use the same electrolyte in all components, different types of electrolytes can be combined in a solid-state battery. A reduction-stable electrolyte can be used on the anode side, while an oxidation-stable electrolyte tailored to the needs of the active cathode material can be used on the cathode side. Here, oxidation stability, conductivity and, of course, cost are the dominant properties that need to be optimized. In all three aspects, aluminium-substituted lithium titanium phosphate (LATP) is a very promising solid Li-ion conductor. This class of materials, first described in 1980,[2] achieves high conductivities in the range of 10^{-4} to 10^{-3} S cm^{-1}. LATP is composed of cheap and abundant elements,[3] has a relatively low density of 2.94 g cm^{-3},[4] is non-flammable and environmentally friendly. LATP has good mechanical stability[5,6] and excellent chemical stability of bulk material to ambient air.[7,8] Although LATP is unstable in direct contact with lithium metal due to the reduction of the Ti^{4+} to Ti^{3+},[9,10] protective coatings for LATP, such as boron nitride, boron oxide, lithium fluoride or magnesium fluoride, have been successfully used in various studies,[11,12] resulting in effective separators. In addition, LATP has been successfully used as a solid electrolyte in mixed cathodes for conventional liquid electrolyte cells,[13] hybrid cells[14–16] and solid-state cells.[17,18] Over the past 30 years, numerous reports have appeared on the optimisation of composition of LATP and its synthesis. Within the $(Li_{1+x}Al_xTi_{2-x}(PO_4)_3)$ system, the best conductivities can be obtained at $0.3 < x < 0.5$.[19] Within this range of lithium and aluminium content, several synthesis routes have proven successful in producing LATP with high ionic conductivities. Additionally, several strategies for doping[20] and sintering additives[6,21,22] have emerged to improve electrochemical performance as well as processability. The maximum

[a]*Institute of Energy and Climate Research – Materials Synthesis and Processing (IEK-1), Forschungszentrum Jülich GmbH, 52425 Jülich, Germany. E-mail: m.finsterbusch@fz-juelich.de*
[b]*Forschungszentrum Jülich GmbH, Institute of Energy and Climate Research, Microstructure and Properties of Materials (IEK-2), 52425 Jülich, Germany*
[c]*Helmholtz Institute Münster: Ionics in Energy Storage (IEK-12), Forschungszentrum Jülich GmbH, Corrensstr. 46, 48149 Münster, Germany*
[d]*Faculty of Engineering and Center for Nanointegration Duisburg-Essen, Universität Duisburg-Essen, Lotharstr. 1, 47057 Duisburg, Germany*
[e]*Chair of Energy Engineering Materials, RWTH Aachen University, 52056 Aachen, Germany*

† Electronic supplementary information (ESI) available. See DOI: https://doi.org/10.1039/d3gc03293k

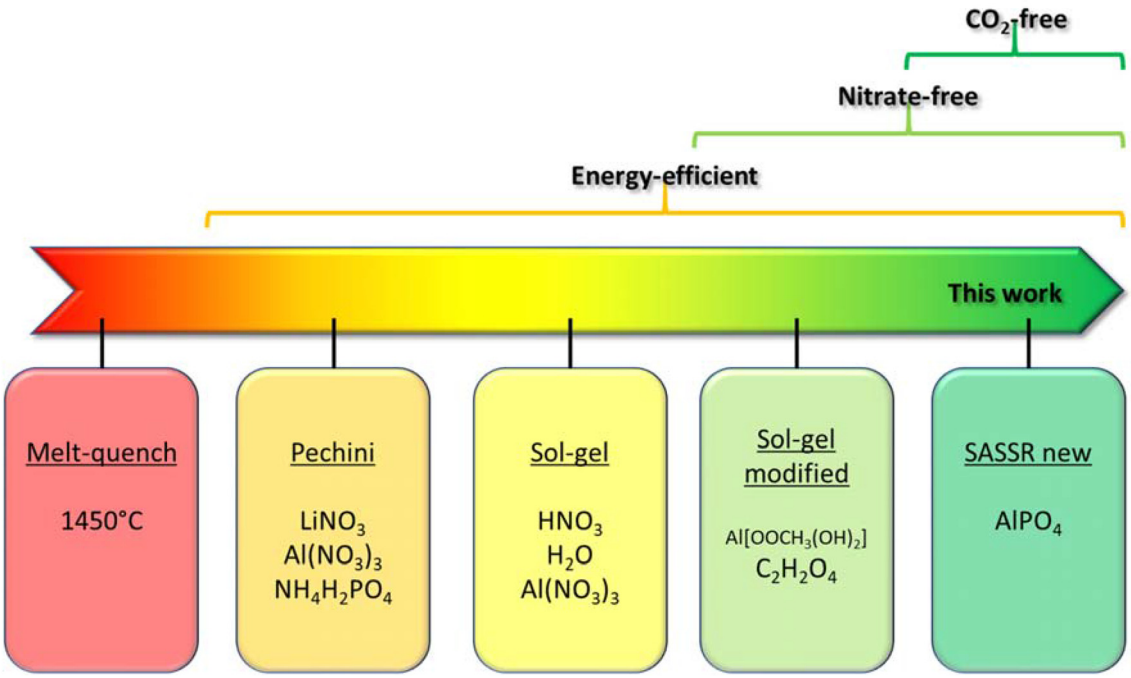

Fig. 1 Evolution of LATP synthesis methods towards high energy efficiency and environmentally benign precursors to reduce the overall ecological footprint of solid-electrolyte production.

total Li-ion conductivities of conventionally sintered LATP pellets at room temperature scatter around 0.6 mS cm^{-1}.[22–28]

Among the possible synthesis methods studied in the last decades, melt-quench synthesis is the oldest. Despite its commercialization, the ionic conductivities of 0.1–0.4 mS cm^{-3} reported for full densified samples[29,30] are rather low. Moreover, not only does it depend on the use of Li_2CO_3, leading to the emission of CO_2 during synthesis, but the melting process at 1450 °C, followed by crushing and resintering at temperatures over 1000 °C, further worsens the environmental impact. Therefore, solution-based processes have taken the lead in recent years. They not only allow easy scale-up of the process but also flexible control of particle size and morphology, which is important for optimizing battery performance.[25,26] In addition to the properties of the resulting powders, the synthesis methods also differ in terms of starting materials, number of synthesis steps, and reaction conditions, which directly affects the economic and environmental impacts. The synthesis routes based on the Pechini method[27,31] and sol–gel synthesis[23,32] rely on water-soluble nitrate precursors, which produce harmful nitrogen oxides as synthesis by-products. To get rid of the nitrogen oxides and improve the environmental performance, a modified sol–gel synthesis was proposed in which the nitrates were replaced by acetate salts.[21] As for the titanium source, titanium isopropoxide has been shown to be the most environmentally friendly option.[21,23,32] Titanium isopropoxide reacts spontaneously with water to form titanium oxide and isopropanol. The isopropanol can be recaptured during the drying step and eventually reused, which improves the sustainability of the process (Fig. 2). However, the acetate ion contained in the aluminium acetate, as well as the oxalic acid stabilising agent, is not recovered but burned to CO_2 during calcination. Further optimization of the environmental impact of the synthesis requires reducing the CO_2 footprint, mainly by finding an alternative aluminium precursor and reducing the amount of organic solvents as well as the energy required during the synthesis.

To further improve the synthesis and drive it towards lower cost and lower environmental impact, we have successfully developed an optimized synthesis route by using aluminium phosphate $AlPO_4$ as a low-cost Al source. The use of aluminium phosphate significantly reduces the need for additional phosphoric acid (H_3PO_4) as P source and eliminates the time-consuming preparation of an aluminium acetate precursor solution.[21]

The resulting synthesis procedure thus requires 12 man-hours less, 43% less energy, and uses fewer and cheaper precursors (10% cost reduction) (ESI Tables 1 and 2†). Most importantly, it presents for the first time a fully carbon neutral synthesis process for LATP, making the solid electrolyte more economical and environmentally friendly (Fig. 1, deep green panel).

Experimental

For the preparation of 100 g of LATP, stoichiometric amounts of lithium hydroxide monohydrate (41.92 g LiOH H_2O, AppliChem, 99+ %), aluminium phosphate (121.94 g $AlPO_4$, Alfa Aesar, 97%) and orthophosphoric acid (97.96 g H_3PO_4, Alfa Aesar, 85%) were added to 1.5 L water. Afterwards, titanium isopropoxide (283.76 g $Ti[OCH(CH_3)_2]_4$, Alfa Aesar, 97+

%) was added dropwise with a rate of 1 mL s^{-1}. The obtained white suspension was stirred for 4 hours at room temperature to ensure homogenization and then dried at 85 °C. Afterwards, the dried precursor powder was homogenized in a planetary ball mill (Retsch PM400) in a 500 ml milling jar with 160 wolfram-carbide milling balls (10 mm) at 300 rpm for 15 minutes and subsequently calcined in a closed Al_2O_3 crucible in air at 600 °C for 5 h, with heating and cooling rates of 5 K min^{-1}. The resulting calcined LATP powder was again milled with the same parameters as mentioned above to prepare for further processing.

The particle size distribution was checked carefully *via* laser diffraction in ethanol using a LA950 (Horiba Scientific) with a 650 nm and a 405 nm laser source. 3 minutes of ultrasonic treatment were applied before measurement to deagglomerate the samples. The data was analysed using a Mie model with a refractive index of 1.54.

To obtain sintered LATP pellets, the calcined and milled powder (LATP-c) as well as the dried and milled educt mixture (LATP-e) was uniaxially pressed into pellets of 13 mm diameter at 75 MPa and sintered in a closed Al_2O_3 crucible at 900 °C for 5 h.

To determine the elemental distribution 50 mg of the sample was melted with 250 mg $Na_2B_4O_7$ at 1050 °C for 30 min. The melt was dissolved in 30 ml 5% HCl and 3 mL H_2O_2 and analysed by ICP-OES (Thermo Scientific iCAP7600). The phase purity was measured *via* X-ray diffraction using a Bruker D4 Endeavor equipped with a 1D detector LYNXEY using monochromatized Cu Ka radiation. Data analysis of the obtained XRD results was carried out by employing the Rietveld method using the software TOPAS (version 6, Bruker AXS, Karlsruhe, Germany). The density of the LATP ceramic was measured by Archimedes' method using deionized and degassed water. A cross-section was cut from the pellets and subsequently embedded in epoxy resin (EpoFix Resin Harz and EpoFix Hardener). The embedded pellet was polished with 4000 grit SiC sand paper and finished with a 1 μm diamond suspension. Powder samples were prepared by attaching the powder to conductive carbon tape. A platinum layer of 1 nm was sputtered onto the sample surface to compensate charging effects. Scanning electron microscopy measurements were taken on a Zeiss EVO 15 (Carl Zeiss AG, Germany) with an acceleration voltage of 15 kV. Energy-dispersive X-ray (EDX) spectra were measured using a Ultim Max 100 detector and analysed using the AZtec software package (both Oxford Instruments plc, England).

Blocking electrodes were applied to the sintered pellets, by sputtering gold onto the fresh surface (2 min sputter time, Cressington 108auto Coater). The impedance was measured in a Swagelok cell using a BioLogic VMP-300 multipotentiostat at 25 °C. The frequency was varied from 7 MHz to 1 Hz with a voltage amplitude of 20 mV. For impedance measurements at elevated and lowered temperatures, two commercial electrochemical systems (Keysight E4991B and Novocontrol Technologies Alpha-A) with an AC frequency range from 3 GHz to 1 MHz and from 10 MHz to 1 Hz were applied, respectively. An alternating voltage amplitude of 20 mV was used during measurements. The temperature dependent impedance was recorded between 433 K and 173 K in a temperature-controlled chamber (Novocontrol Technologies BDS1100). The data analysis and fitting were performed with the EC-lab software (Biologic, V11.36). All graphs were normalized to the thickness and area of the samples. The conductivities were calculated using the formula $\sigma = \frac{d}{RA}$, where R is the resistance, d is the sample thickness and A is the sample area. The activation energy E_a was determined from a linear fit of the Arrhenius plot according to the Arrhenius equation $\sigma T \sim \exp\left(\frac{-E_a}{kT}\right)$, where σ is the ionic conductivity, k is the Boltzmann constant and T is the absolute temperature.

Results and discussion

Economical and ecological impact

The choice of starting materials is considered fundamental to the phase purity and morphology of the LATP powder[33] (see Fig. 1, red to light green panel). In general, water-soluble starting materials are chosen to ensure homogeneous distribution of all elements. In an optimized process reported previously,[32,33] lithium hydroxide, phosphoric acid, titanium isopropoxide, and aluminium acetate were used as precursors to obtain LATP powder with the highest ionic conductivity. All compounds have good ecological fingerprint except aluminium acetate as described above. Therefore, the focus of this work was to replace aluminium acetate with an alternative aluminium source to minimize CO_2 emissions.

The synthesis of LATP in the synthesis route used as the basis for modifications[21] was carried out in a modified solution-assisted solid-state reaction (SASSR) consisting of three main steps (Fig. 2, left). First, an aluminium acetate solution is prepared, and the aluminium content is checked. In the mixing step, the stoichiometric amount of LATP precursors is stirred in water and then dried at 85 °C. The dried product is ball milled and calcined in a calcination step at 600 °C to remove the volatiles. The result is an amorphous LATP powder that can then be sintered at temperatures >900 °C to obtain crystalline LATP with high ionic conductivity. The sintering temperature required for this process depends critically on the particle size and particle size distribution of the amorphous LATP powders obtained in the calcination step, with smaller particles allowing lower sintering temperatures.

To reduce the carbon footprint of LATP synthesis, carbon-containing anions must be excluded from the high-temperature processing steps. Ideally, all anions other than phosphate ions should be avoided to simplify the reaction mixture composition and avoid the formation of additional by-products. As aluminium acetate is the only CO_2 source in the synthesis route used as standard in our work (Fig. 2, left),[21] replacing the acetate ion with the phosphate would result in aluminium phosphate $AlPO_4$.

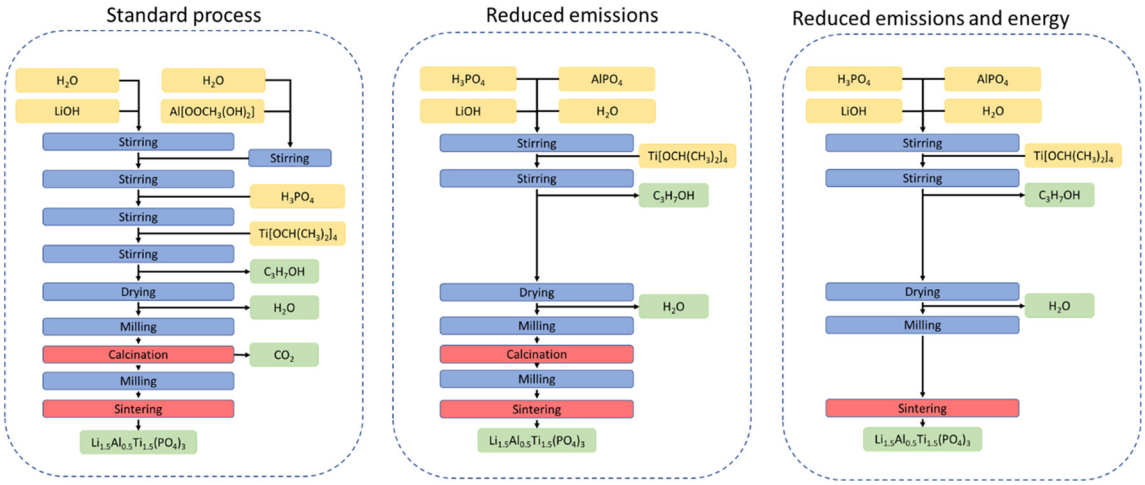

Fig. 2 Flowchart of the LATP synthesis routes under consideration. Left: standard SASSR synthesis as described by B. Davaasuren and F. Tietz;[21] middle: optimized SASSR synthesis with reduced CO2 emissions using carbon-free Al source (LATP-c); right: further optimization of the LATP-c synthesis omitting the calcination steps (LATP-e).

This new synthesis method follows the reaction

$$1.5\mathrm{Ti[OCH(CH_3)_2]_4} + 3\mathrm{H_2O} \rightarrow 1.5\mathrm{TiO_2} + 6\mathrm{CH_3H_8O}$$

$$1.5\mathrm{LiOH} + 0.5\mathrm{AlPO_4} + 1.5\mathrm{TiO_2} + 0.5\mathrm{H_3PO_4} \rightarrow \mathrm{Li_{1.5}Al_{0.5}Ti_{1.5}(PO_4)_3} + 4.5\mathrm{H_2O}$$

Besides the lower carbon footprint, the advantage of $AlPO_4$ is that it is cheap and commercially available. In addition, the reaction is simplified because the aluminium-source does not need to be prepared as solution separately. To test the suitability of $AlPO_4$ as an Al source, it was added to the reaction mixture described above. The rest of the synthesis procedure was carried out under otherwise similar conditions to prepare LATP-c powder (Fig. 2, middle), as TGA measurements indicated the start of the phase formation reaction at 530 °C (ESI Fig. 1†). In addition, a second synthesis route is proposed here in which the reactant mixture is directly sintered and the high-temperature calcination step is completely omitted (Fig. 2, right). To evaluate the improvement by these modifications to the ecological and economical impact of the synthesis, the data basis of existing literature is insufficient. Since the environmental impact of battery material synthesis has not been a focus in reports of new synthesis methods so far, critical data, such as the amount of additives needed or the exact energy input have not been reported consistently. Therefore, the solution-assisted solid-state reaction based on aluminium-acetate has been recreated to create the data base for comparison (ESI Tables 1 and 2†).

The substitution of the aluminium source in the synthesis process of LATP eradicates CO_2 emissions from the reactants, while the required input of H_3PO_4 is reduced by 64 g kg^{-1} LATP. Moreover, these savings lead to a 10% reduction in the price of the required materials. In addition, the proposed shortened process leads to a significant reduction in labour hours and electrical energy consumption. In the production of LATP-c, 8 labour hours are saved, while energy use is reduced by 19% or 9 kW h kg^{-1} LATP, which is equivalent to 3790 g CO_2 per kg LATP. For the production of LATP-e, the savings are even higher, as the number of labour hours is reduced by 12, while the energy input is reduced by 43% or 21 kW h kg^{-1} LATP, equivalent to 8820 g CO_2 per kg LATP. Even though these figures only apply to laboratory-scale production, as the commercial process is not yet established, they show the immense economic and ecological potential of the processing method presented here.

Material characterization and electrochemical performance

To prove the competitiveness of the proposed synthesis routes, a thorough analysis of the obtained materials is required. After drying and calcination, an amorphous LATP-c powder was obtained, which showed a bimodal particle size distribution with a relatively broad distribution around 10 μm and a narrow distribution at 0.1 μm after the dry milling process (Fig. 3). The narrow distribution of the smaller particle fraction with a small amount of larger particles is generally beneficial for further sintering and densification, as it leads to high green body densities.[34] Since the particle and crystallite size can easily be easily adjusted and there is no evolution of gases in subsequent processing, the LATP powder produced by this method is suitable also for advanced sintering techniques such as spark plasma sintering.[4,29,35]

The second synthesis route proposed in this work (LATP-e) is based on the direct sintering of the mixed reactants. In this case, the phase purity and electrochemical properties of the obtained LATP-e pellets depend on the particle size and the particle size distribution of the reactants, which can be adjusted to achieve the desired material properties. Scanning electron microscopy (SEM) images of LATP-c and LATP-e powders (Fig. 3c and d) show that both materials have comparable morphology consisting of spherical agglomerates with

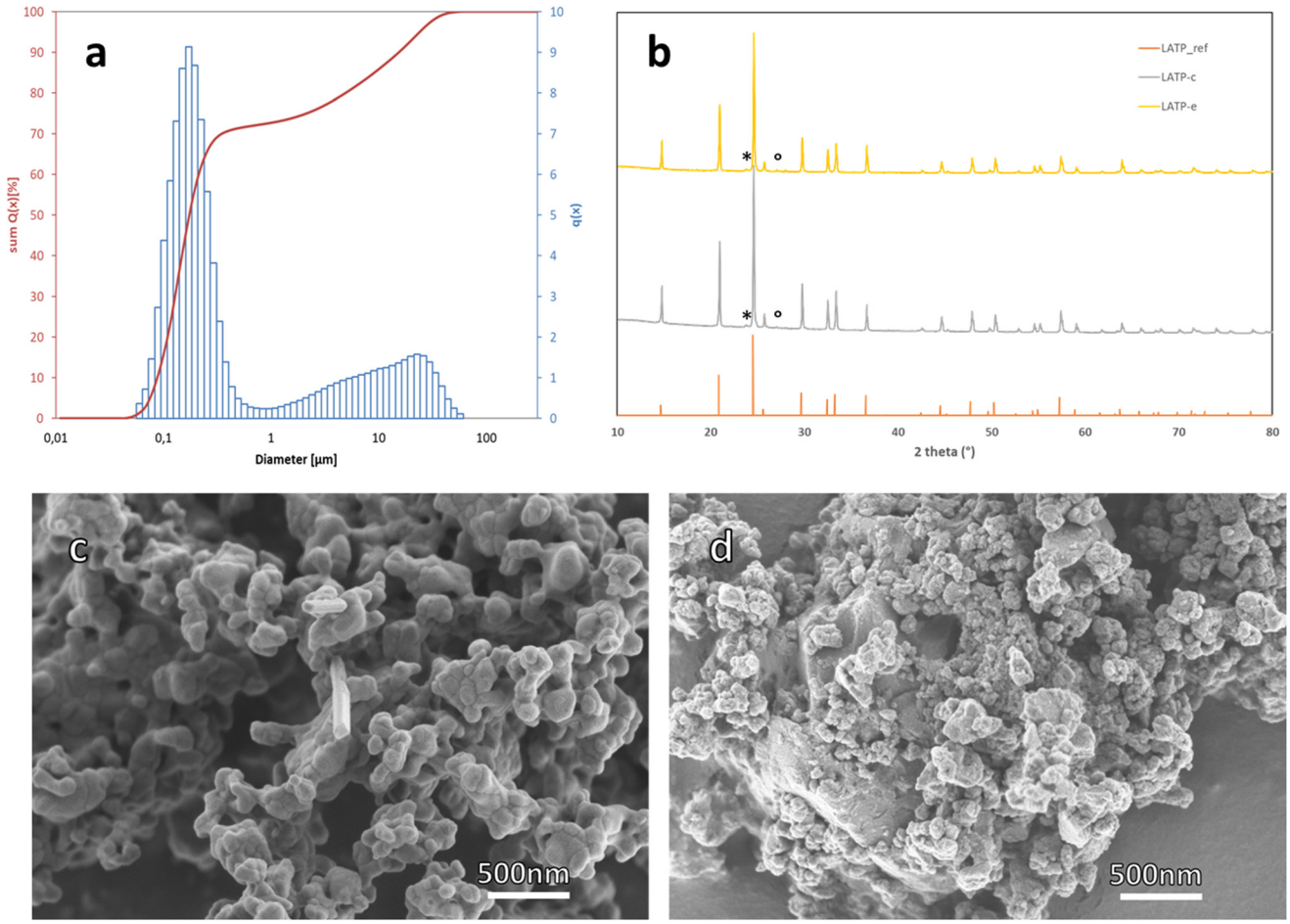

Fig. 3 (a) Particle size distribution of LATP-c powder after final dry milling; (b) XRD data of LATP-c (grey) und LATP-e (yellow); orthorhombic LATP phase marked as *; LTP phase marked as °; (c) SEM picture of the calcined LATP-c powder after wet milling and drying; (d) SEM picture of the reactant mixture in LATP-e synthesis after wet milling and drying.

similar size of primary particles, as well as larger polycrystalline particles (ESI Fig. 2†).

To test the sintering performance of the LATP-e powder and the calcined LATP-c powder, as well as the phase purity of the resulting LATP solid electrolyte, both powders were uniaxially pressed into pellets and sintered at 900 °C for 5 h. The composition of the synthesized was determined *via* ICP-OES (ESI Table 3†). Both LATP-c and LATP-e are within the measurement accuracy of the method similar to the target composition of $Li_{1.5}Al_{0.5}Ti_{1.5}P_3$. X-ray diffraction (XRD) analysis (Fig. 3b) and Rietveld refinement (ESI Fig. 3 and 4†) of the sintered pellet show the formation of crystalline LATP with high phase purity. The majority of the material (94 wt% for LATP-c and 93 wt% for LATP-e) consists of LATP with a targeted rhombohedral phase configuration (space group $R\bar{3}c$, ICSD 7936). A small amount of LATP (4 wt% for LATP-c and 5 wt% for LATP-e) crystallizes in the orthorhombic phase structure (space group *Pbca*, structure similar to that of $Li_2Mn_2(SO_4)_3$ type, ICSD 51332, indicated by asterisks (*) in Fig. 3d) first reported by Gross *et al.*[6] and observed in virtually all reported LATP materials. While the occurrence of this orthorhombic LATP has been associated with sintering temperature, its effect on the electrochemical stability and ionic conductivity is still unclear. In addition, a very small amount (2 wt% for LATP-c and LATP-e) of an Al-poor $LiTiPO_5$ phase, indicated by °, was detected as a secondary phase. The phase purity of our crystalline LATP is higher than that of LATP materials prepared by other reported synthesis methods,[5,21,30] which report secondary phases with 3 wt% to 10 wt%. It should also be noted that this high phase purity was achieved at a temperature of only 900 °C, which is among the lowest sintering temperatures reported for this material. It is also noteworthy that no secondary $AlPO_4$ phase can be detected in our LATP, although $AlPO_4$ is a reactant in this new synthesis route, proving its complete consumption during the synthesis process. This is particularly noteworthy since in several other reports[11,12,21,29,33,35] where $AlPO_4$ was not used as a source of aluminium, $AlPO_4$ was still reported as a secondary phase. The $AlPO_4$ impurity phase has been shown to have a particularly detrimental effect on the subsequent processing of LATP, leading, for example, to the formation of cracks during pressure-assisted sintering.[29]

In addition to the high phase purity, the sintered LATP pellets produced from calcined powders exhibit a sufficiently high relative density of 90% (determined by the Archimedes method). When considering only conventionally sintered LATP without additives, the reported range of relative densities is between 87% and 95%,[23,24,36,37] for competitive conductivities.

Scanning electron microscopy (SEM) images of the polished cross-section of the sintered pellets show a dense microstructure with small pores (Fig. 4). Energy-dispersive X-ray (EDX) spectra show an overall uniform element distribution (ESI Fig. 5 and 6†), with only some isolated small grains having a significantly lower Al concentration (Fig. 5 and ESI Fig. 6†). The chemical composition of these inclusions agrees well with the secondary $LiTiPO_5$ phase detected in the XRD. This otherwise detrimental secondary phase does not cover the grain boundaries and consequently has no significant negative impact on the electrochemical performance of our material.

Finally, ionic conductivity, the most important property of a solid electrolyte, was determined on sintered pellets by impedance spectroscopy. Due to the semi-blocking nature of the gold electrode, the low-frequency region of the graph displays the sluggish alloying reaction between lithium and gold. The Nyquist plot of the impedance spectrum at 25 °C (Fig. 6a and c) shows a semicircle in the mid-frequency range attributed to grain boundary resistance, with a capacitance of 3×10^{-9} F for LATP-c and 1.5×10^{-9} F for LATP-e. A semicircle attributed to bulk material resistance, normally observed at high frequencies, was not observed in the frequency range used at room temperature. Therefore, the bulk conductivity was calculated from the high-frequency intercept of the semicircle on the x-axis as σ_{bulk} 2.5 mS cm^{-1}, which is in good agreement with bulk conductivity data obtained on single crystals.[38] At lowered temperatures, a distinct semi-circle with a capacitance of 25×10^{-12} F, attributed to the bulk resistance, can be seen in the high frequency range (ESI Fig. 7†). While this indicates

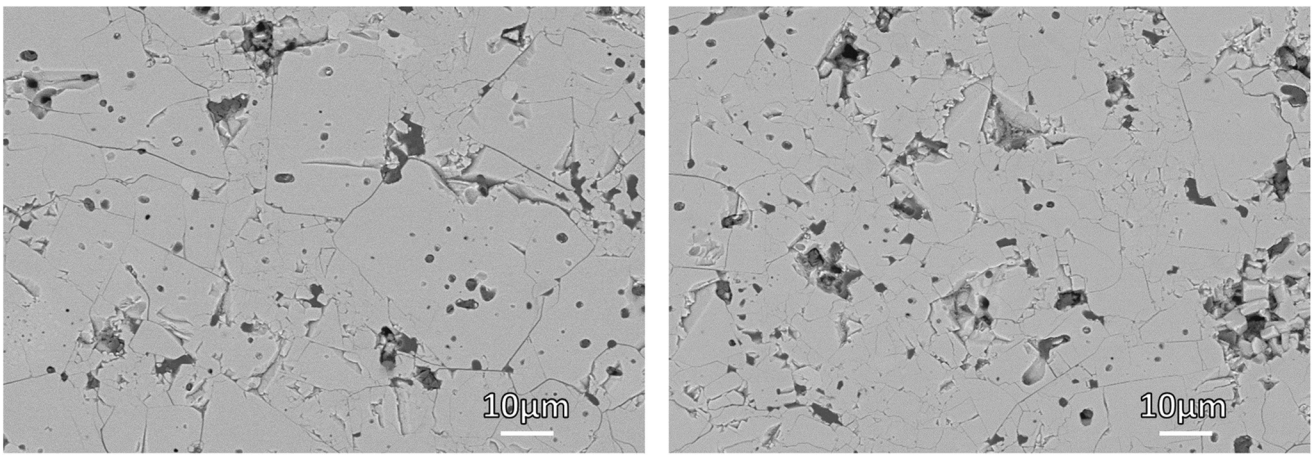

Fig. 4 SEM picture of a polished cross-section of the sintered pellets of LATP-c (left) and LATP-e (right).

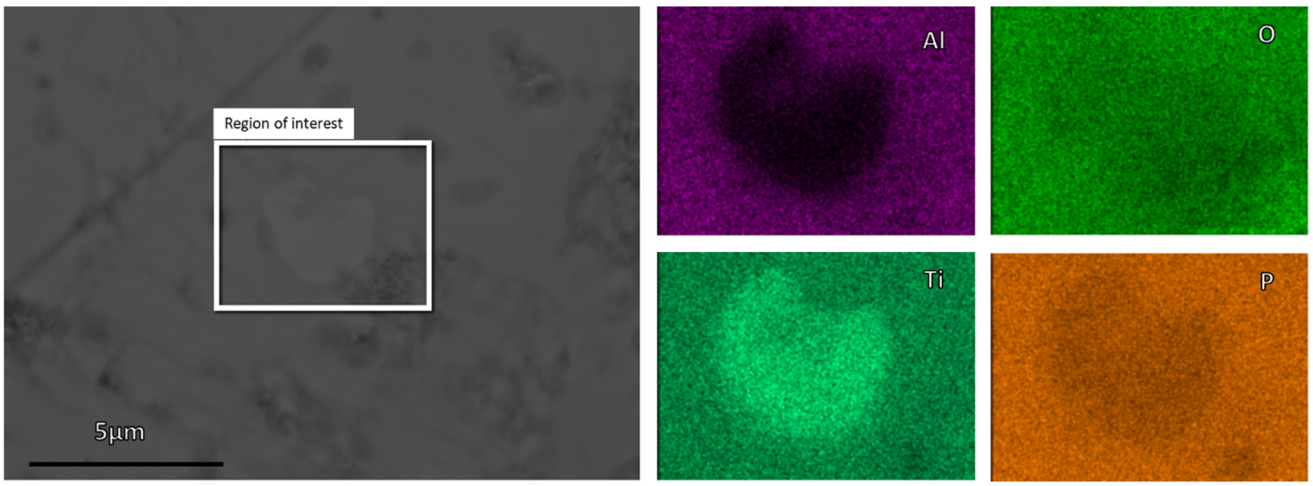

Fig. 5 SEM of the polished cross-section of sintered LATP-c pellets; EDX the marked area of sintered LATP-c pellets.

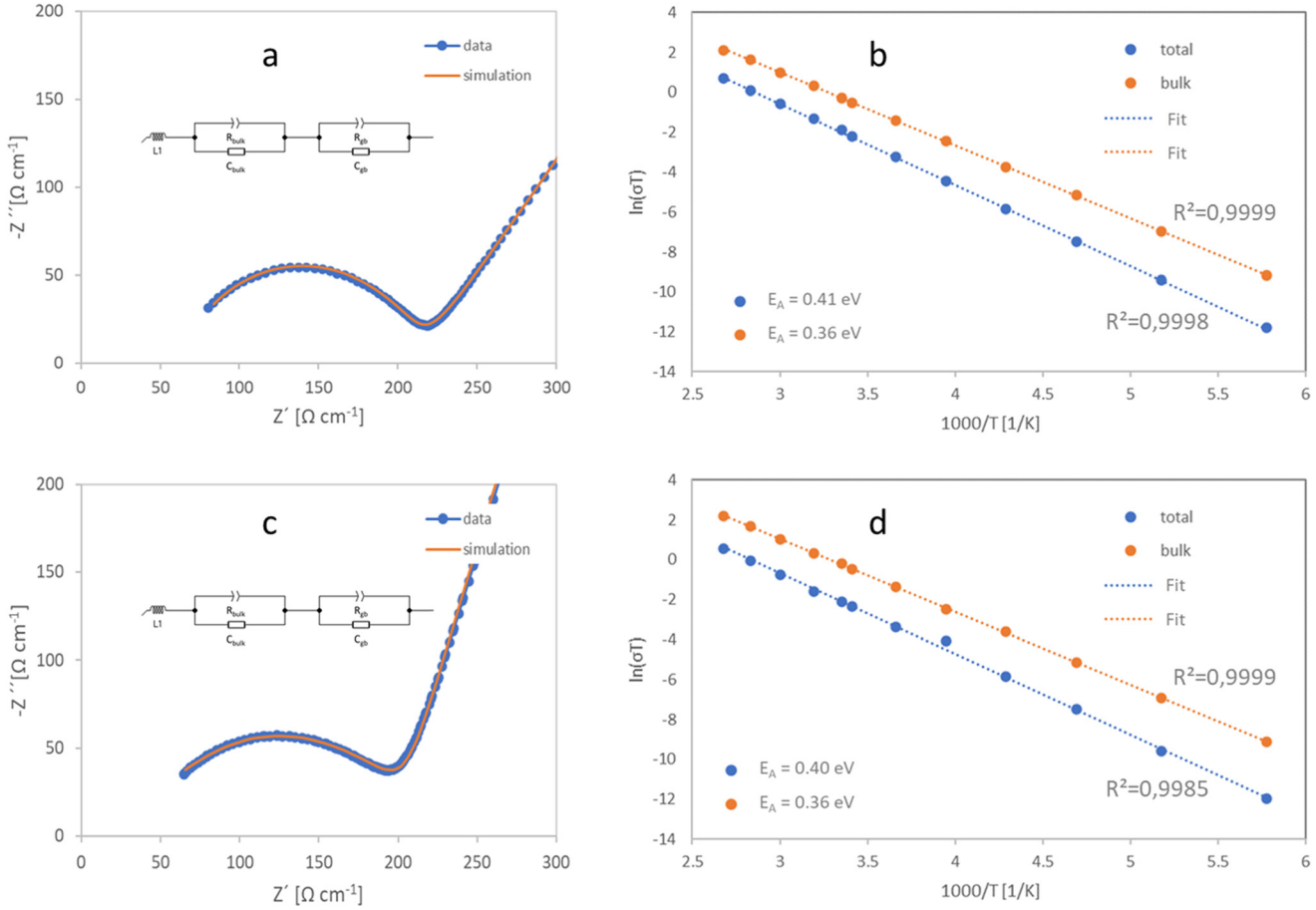

Fig. 6 (a) Nyquist plot of the room temperature impedance measurement of the sintered LATP-c pellet, (b) Arrhenius plot of ionic conductivities of the sintered LATP-c pellets in the temperature range –100 °C to 100 °C, (c) Nyquist plot of the room temperature impedance measurement of the sintered LATP-e pellet (d) Arrhenius plot of ionic conductivities of the sintered LATP-e pellets in the temperature range –100 °C to 100 °C.

sufficient phase purity, the total conductivity of LATP is generally governed by the grain boundary resistance.[5] The total conductivity (bulk + grain boundary) is determined as σ_{tot} = 0.62 mS cm^{-1} at 25 °C LATP-c and as σ_{tot} = 0.59 mS cm^{-1} at 25 °C for LATP-e from the data-fit. These values prove the competitiveness of the presented synthesis routes, as the highest conductivities for conventionally sintered LATP scatter around 0.6mS cm^{-1}.[22–28] Impedance measurements were also performed at different temperatures to determine the activation energy E_a for Li-ion transfer (Fig. 6b and d). Both LATP-c and LATP-e exhibit a relatively low activation energy (total activation energy of 0.41 eV and 0.40 eV for LATP-c and LATP-e, respectively, and the bulk activation energy of 0.36 eV), which is comparable to the activation energy of LATP obtained in the aluminium acetate-based synthesis route (0.41 eV total activation energy).[23]

Conclusions

In this work, we present a new simplified process for the preparation of high quality LATP *via* a modified SASSR route. A competitive total ion conductivity of 0.62 mS cm^{-1} at room temperature was achieved by conventional free sintering at 900 °C, resulting in a sample with 90% relative density. The phase purity, relative density, ionic conductivity, and ion transport activation energy values of our LATP are comparable to those of LATP prepared by other methods such as sol–gel synthesis[23] or molten flux-assisted solid-state synthesis.[25] However, similar or even better performance was achieved in a much simpler process with less expensive starting materials, demonstrating the competitiveness of our new synthesis methods. By using aluminium phosphate as the Al source in the SASSR process presented here, the amount of orthophosphoric acid and CO_2 emissions from reactants and energy emissions were significantly reduced. This not only reduces the environmental impact of LATP synthesis, but also significantly lowers synthesis cost, further driving LATP towards the large-scale application.

Author contributions

Writing – original draft: M. R.; writing – review& editing: P. H., M. M., Q. M., J. G., M. F., O. G. and D. F.; investigation:

M. R. and P. H.; formal analysis: J. G. and M. M.; funding acquisition: M. F., D. F. and O. G.; project administration: M. F.; conceptualization: M. R., M. F. and D. F.

Conflicts of interest

There are no conflicts to declare.

Acknowledgements

Financial support by the German Federal Ministry of Education and Research (BMBF) as part of the clusters of competency Festbatt 2 (projects 13XP0434A and 13XP0432B) and EProFest (13XP0346B) is gratefully acknowledged.

References

1 J. Janek and W.G. Zeier, *A solid future for battery development*, in *Nature Energy*, Macmillan Publishers Limited, 2016, vol. 1, p. 1–4.
2 H. Aono, E. Sugimoto, Y. Sadaoka, N. Imanaka and G. Adachi, Ionic Conductivity of the Lithium Titanium Phosphate Systems, *J. Electrochem. Soc.*, 1989, **136**(2), 590–591.
3 Mineral commodity summaries 2023, U.S. Geological Survey, p. 210.
4 E. C. Bucharsky, K. G. Schell, A. Hintennach and M. J. Hoffmann, Preparation and characterization of sol–gel derived high lithium ion conductive NZP-type ceramics $Li_{1+x}Al_xTi_{2-x}(PO_4)_3$, *Solid State Ionics*, 2015, **274**, 77–82.
5 S. D. Jackman and R. A. Cutler, Effect of microcracking on ionic conductivity in LATP, *J. Power Sources*, 2012, **218**, 65–72.
6 J. P. Gross, J. Malzbender, E. Dashjav, F. Tietz and R. Schwaiger, Conductivity, microstructure and mechanical properties of tape-cast LATP with LiF and SiO_2 additives, *J. Mater. Sci.*, 2022, **57**(2), 925–938.
7 S. Hasegawa, N. Imanishi, T. Zhang, J. Xie, A. Hirano, Y. Takeda, *et al.*, Study on lithium/air secondary batteries-Stability of NASICON-type lithium ion conducting glass-ceramics with water, *J. Power Sources*, 2009, **189**(1), 371–377.
8 E. Dashjav, Q. Ma, Q. Xu, C. L. Tsai, M. Giarola, G. Mariotto, *et al.* The influence of water on the electrical conductivity of aluminum-substituted lithium titanium phosphates, *Solid State Ionics*, 2018, **321**, 83–90.
9 Y. Zhu, X. He and Y. Mo, Origin of Outstanding Stability in the Lithium Solid Electrolyte Materials: Insights from Thermodynamic Analyses Based on First-Principles Calculations, *ACS Appl. Mater. Interfaces*, 2015, **7**(42), 23685–23693.
10 P. Hartmann, T. Leichtweiss, M. R. Busche, M. Schneider, M. Reich, J. Sann, *et al.*, Degradation of NASICON-type materials in contact with lithium metal: Formation of mixed conducting interphases (MCI) on solid electrolytes, *J. Phys. Chem. C*, 2013, **117**(41), 21064–21074.
11 L. Zhu, Y. Wang, Y. Wu, W. Feng, Z. Liu, W. Tang, *et al.*, Boron Nitride-Based Release Agent Coating Stabilizes $Li_{1.3}Al_{0.3}Ti_{1.7}(PO_4)_3$/Li Interface with Superior Lean-Lithium Electrochemical Performance and Thermal Stability, *Adv. Funct. Mater.*, 2022, **32**(29), 2201136.
12 L. Yang, Y. Song, H. Liu, Z. Wang, K. Yang, Q. Zhao, *et al.*, Stable Interface between Lithium and Electrolyte Facilitated by a Nanocomposite Protective Layer, *Small Methods*, 2020, **4**(3), 1–7.
13 C. C. Yang, J. R. Jiang, C. Karuppiah, J. H. Jang, Z. H. Wu, R. Jose, *et al.*, LATP ionic conductor and in-situ graphene hybrid-layer coating on $LiFePO_4$ cathode material at different temperatures, *J. Alloys Compd.*, 2018, **765**, 800–811.
14 M. Ihrig, E. Dashjav, A. M. Laptev, R. Ye, D. Grüner, M. Ziegner, *et al.*, Increasing the performance of all-solid-state Li batteries by infiltration of Li-ion conducting polymer into LFP-LATP composite cathode, *J. Power Sources*, 2022, **543**, 231822.
15 H. Zhai, T. Gong, B. Xu, Q. Cheng, D. Paley and B. Qie, Stabilizing Polyether Electrolyte with a 4 V Metal Oxide Cathode by Nanoscale Interfacial Coating, *ACS Appl. Mater. Interfaces*, 2019, **11**(32), 28774–28780.
16 X. Ban, W. Zhang, N. Chen and C. Sun, A High-Performance and Durable Poly(ethylene oxide)-Based Composite Solid Electrolyte for All Solid-State Lithium Battery, *J. Phys. Chem. C*, 2018, **122**(18), 9852–9858.
17 Q. Xu, Z. Liu, A. Windmüller, S. Basak, J. Park, K. Dzieciol, *et al.*, Active Interphase Enables Stable Performance for an All-Phosphate-Based Composite Cathode in an All-Solid-State Battery, *Small*, 2022, **18**(21), 2200266.
18 K. Nagata and T. Nanno, All solid battery with phosphate compounds made through sintering process, *J. Power Sources*, 2007, **174**(2), 832–837.
19 G. J. Redhammer, D. Rettenwander, S. Pristat, E. Dashjav, C. M. N. Kumar, D. Topa, *et al.*, A single crystal X-ray and powder neutron diffraction study on NASICON-type $Li_{1+x}Al_xTi_{2-x}(PO_4)_3$ ($0 \leq x \leq 0.5$) crystals: Implications on ionic conductivity, *Solid State Sci.*, 2016, **60**, 99–107.
20 S. Li, Z. Huang, Y. Xiao and C. Sun, Chlorine-doped $Li_{1.3}Al_{0.3}Ti_{1.7}(PO_4)_3$as an electrolyte for solid lithium metal batteries, *Mater. Chem. Front.*, 2021, **5**(14), 5336–5343.
21 B. Davaasuren and F. Tietz, Impact of sintering temperature on phase formation, microstructure, crystallinity and ionic conductivity of $Li_{1.5}Al_{0.5}Ti_{1.5}(PO_4)_3$, *Solid State Ionics*, 2019, **338**, 144–152.
22 L. Dai, J. Wang, Z. Shi, L. Yu and J. Shi, Influence of $LiBF_4$ sintering aid on the microstructure and conductivity of LATP solid electrolyte, *Ceram. Int.*, 2021, **47**(8), 11662–11667.
23 Q. Ma, Q. Xu, C. L. Tsai, F. Tietz and O. Guillon, A Novel Sol-Gel Method for Large-Scale Production of Nanopowders: Preparation of $Li_{1.5}Al_{0.5}Ti_{1.5}(PO_4)_3$ as an Example, *J. Am. Ceram. Soc.*, 2016, **99**(2), 410–414.

24 J. Liu, T. Liu, Y. Pu, M. Guan, Z. Tang, F. Ding, *et al.*, Facile synthesis of NASICON-type $Li_{1.3}Al_{0.3}Ti_{1.7}(PO_4)_3$ solid electrolyte and its application for enhanced cyclic performance in lithium ion batteries through the introduction of an artificial Li3PO4 SEI layer, *RSC Adv.*, 2017, **7**(74), 46545–46552.

25 L. Xingang, T. Jiang, J. Fu, R. Yuan, H. Wen and C. Zhang, Facile Synthesis of Nanosized Lithium-Ion-Conducting Solid Electrolyte $Li_{1.4}Al_{0.4}Ti_{1.6}(PO_4)_3$ and Its Mechanical Nanocomposites with $LiMn_2O_4$ for Enhanced Cyclic Performance in Lithium Ion Batteries, *ACS Appl. Mater. Interfaces*, 2017, **9**(13), 11696–11703.

26 B. Yang, X. Li, H. Guo, Z. Wang and W. Xiao, Preparation and properties of $Li_{1.3}Al_{0.3}Ti_{1.7}(PO_4)_3$ by spray-drying and post-calcining method, *J. Alloys Compd.*, 2015, **643**, 181–185.

27 E. Zhao, F. Ma, Y. Jin and K. Kanamura, Pechini synthesis of high ionic conductivity $Li_{1.3}Al_{0.3}Ti_{1.7}(PO_4)_3$ solid electrolytes: The effect of dispersant, *J. Alloys Compd.*, 2016, **680**, 646–653, DOI: **10.1016/j.jallcom.2016.04.173**.

28 N. V. Kosova, E. T. Devyatkina and A. P. Stepanov, Lithium conductivity and lithium diffusion by mechanical activation, *Ionics*, 2008, **14**, 303–311.

29 K. Waetzig, A. Rost, C. Heubner, M. Coeler, K. Nikolowski, M. Wolter, *et al.*, Synthesis and sintering of $Li_{1.3}Al_{0.3}Ti_{1.7}(PO_4)_3$ (LATP) electrolyte for ceramics with improved Li+ conductivity, *J. Alloys Compd.*, 2020, **818**, 153237.

30 E. C. Bucharsky, K. G. Schell, T. Hupfer, M. J. Hoffmann, M. Rohde and H. J. Seifert, Thermal properties and ionic conductivity of $Li_{1.3}Ti_{1.7}Al_{0.3}(PO_4)_3$ solid electrolytes sintered by field-assisted sintering, *Ionics*, 2016, **22**(7), 1043–1049.

31 M. R. Ghaani, A. M. Mohtasebi, R. Tajeri and P. Marashi, A comparison of the role of the chelating agent on the structure of lithium conducting solid electrolyte li1.4al0.4ti1.6 (po4)3: Pechini vs. modified pechini-type methods, *Batteries*, 2020, **6**(4), 1–13.

32 M. Kotobuki and M. Koishi, Preparation of $Li_{1.3}Al_{0.3}Ti_{1.7}(PO_4)_3$ solid electrolyte via a sol-gel method using various Ti sources, *J. Asian Ceram. Soc.*, 2020, **8**(3), 891–897.

33 M. Kotobuki and M. Koishi, Preparation of $Li_{1.5}Al_{0.5}Ti_{1.5}(PO_4)_3$solid electrolyte via a sol-gel route using various Al sources, *Ceram. Int.*, 2013, 4645–4649.

34 M. N. Rahaman, *Ceramic processing and sintering*, CRC press, 2003.

35 X. Xu, Z. Wen, X. Yang and L. Chen, Dense nanostructured solid electrolyte with high Li-ion conductivity by spark plasma sintering technique, *Mater. Res. Bull.*, 2008, **43**(8–9), 2334–2341.

36 K. Waetzig, A. Rost, C. Heubner, M. Coeler, K. Nikolowski, M. Wolter, *et al.*, Synthesis and sintering of $Li_{1.3}Al_{0.3}Ti_{1.7}(PO_4)_3$ (LATP) electrolyte for ceramics with improved Li+ conductivity, *J. Alloys Compd.*, 2020, **818**, 153237.

37 E. Zhao, F. Ma, Y. Jin and K. Kanamura, Pechini synthesis of high ionic conductivity $Li_{1.3}Al_{0.3}Ti_{1.7}(PO_4)_3$ solid electrolytes: The effect of dispersant, *J. Alloys Compd.*, 2016, **680**, 646–653.

38 D. Rettenwander, A. Welzl, S. Pristat, F. Tietz, S. Taibl, G. J. Redhammer, *et al.*, A microcontact impedance study on NASICON-type $Li_{1+x}Al_xTi_{2-x}(PO_4)_3 (0 \leq x \leq 0.5)$ single crystals, *J. Mater. Chem. A*, 2016, 1506–1513.